Design of Contact Compliance and Simulation of Touch-Down Sequence of MUSES-C Spacecraft for Asteroid Sampling

Kazuya Yoshida
Department of Aeronautics and Space Engineering, Tohoku University
Aoba 01, Sendai 980-8579, Japan
yoshida@astro.mech.tohoku.ac.jp

Abstract

Small planetary objects such as asteroids and comets receive increasing attention for near-future exploration of the solar system. Some pioneering probes have already sent and returned remarkable findings, and others are being planned and developed to follow them. In Japan, the Institute of Space and Astronautical Science (ISAS), is now organizing the development of a sample-return mission to an asteroid. A spacecraft named MUSES-C is targeting one of near-Earth asteroids, in order to obtain samples and return to Earth. Robotics technologies are applied to the guidance and control of the landing and contact. Since the gravity of the asteroid is very small, the spacecraft will not be able to stand on its surface, but make dynamic touch in a free-flying situation. In this paper, the free-flying and contact dynamics are investigated to study the touch-down sequence for sample acquisition. The contact with mechanical compliance is modeled and dynamics simulations are carried out for feasible touch-down conditions.

1 Introduction

Asteroids are small particles of rocky bodies orbiting the Sun, a concentration of which bodies form an asteroid belt between Mars and Jupiter. The investigation into the astronomical questions on where these bodies come from, why they concentrate there, and what materials they are composed of, brings us significant knowledge on the origin and history of our solar system. The most informative way to answer these questions is to obtain samples from these planetary bodies themselves.

The Institute of Space and Astronautical Science (ISAS), Japan has a plan to launch an exploration robotic spacecraft, named MUSES-C, which can touch down on a surface of an asteroid and acquire samples off its surface, then take them back to the Earth [1]. In a tentative mission scenario, MUSES-C, a 400 [kg] spacecraft, will target one of the near earth asteroids, estimated less than 1 [km] diameter rocky object. Candidates for such asteroids are "NEREUS" and "1989ML." The MUSES-C approaches to the asteroid's surface with small relative velocity controlled by a vision-based guiding system and makes contact by a horn-like sampling probe. Inside the probe, a projectile is projected toward the planet with some high velocity to crash the surface, then rebounding particles, ejecta, will be collected at the top corner of the horn.

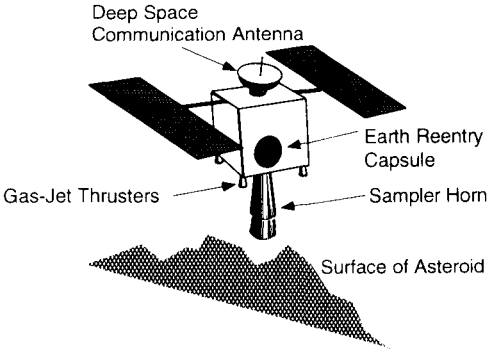

Figure 1: The asteroid sample-return spacecraft, MUSES-C

There are many technical challenges in this mission. Particularly contact with the surface of asteroid is one of the most critical challenges. In order to make sure the safety, in terms of the strength of the structure against the impulsive force and the attitude maintenance against the impulsive moment, we need to carefully design the mechanisms and control systems, and simulate their dynamic behavior with making use of our maximum knowledge on the free-flying and contact dynamics. Only limited experiments are possible to test micro-gravity environment on Earth, thus hardware verification with a full-scale model is usually very difficult. Computer simulations are therefore a significant approach to study this design problem.

This paper discusses the dynamic simulation of

Proc. Fifth International Symposium on Artificial Intelligence, Robotics and Automation in Space, 1-3 June 1999 (ESA SP-440)

the touch-down sequence with the development of free-flying and contact models then, using tentative design parameters of MUSES-C, illustrates the dynamic motion after the contact.

2 MUSES-C Mission Scenario

2.1 MUSES-C

MUSES-C is a spacecraft for the asteroid sampling-return mission which is planned by ISAS to launch in 2002. Figure 1 depicts a basic configuration of the spacecraft, with 400 [kg] total mass and the dimension of the main body: 1.6[m] × 1.0[m] × 1.0[m]. The spacecraft has the following subsystems: an ion engine system for interplanetary voyage, a high-gain antenna for deep space communication, solar paddles, thruster propulsion systems, a sampling mechanism called "sampler horn" and a reentry capsule back to Earth. After the sampling action, sample particles are collected and packed into the reentry capsule, then its door is latched and sealed carefully to avoid contamination. When the spacecraft returns to Earth, only the reentry capsule, which we hope filled with a lot of informative samples, parachutes down to the Earth's surface.

2.2 Asteroids

Asteroids are small particles of rocky bodies orbiting the Sun. Up to now, we have a very limited information about these small planets through telescopes, and analysis of meteors. Recently, impressive pictures of some asteroids are taken by deep space explorers, such as Galileo. Those pictures show that an asteroid is not a spherical planet but a very oblique and rugged rock with craters. Generally speaking, these images agree our scientific expectation in the point that, for example, the gravity is not strong enough to form a spherical planet in these size of objects. But specific information such that, if an asteroid is a huge monolith or a cluster of soft soils, if the surface is rocky, sandy or dusty, and what materials it is composed of... all these are open questions, and the answers depend on the history of each asteroid.

In a tentative mission scenario, MUSES-C will target the asteroid NEREUS, or 1989ML. So far our knowledge is very limited on these asteroids, particularly its gravity and the surface condition (hardness, roughness), and right answers should be given only when the MUSES-C makes a physical contact with it. For the purpose of the simulation study, we assume the gravity on surface 9.8×10^{-4} [m/s^2].

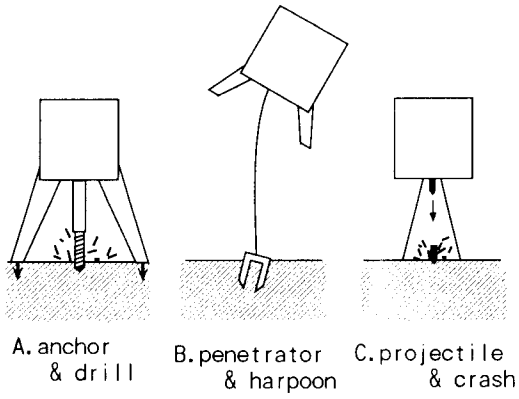

Figure 2: Sampling Methods

2.3 Sampling Strategy

In order to obtain samples from a small planet, which does not have enough gravity to firmly fix the explorer on its surface, the following strategies depicted in Figure 2 have been discussed.

Drilling technology (A) may work effectively for the sampling from a comet, which is considered to be composed of relatively *soft* materials such as dusty, icy, and snowy compounds. However an asteroid is considered as a more rocky or stony object covered with relatively *hard* surface, then we need more high-energy methods to crash the surface.

One of such methods is with a penetrator harpoon (B). If a penetrator capsule is projected down to a planet, it will be packed with crashed surface materials. In this method, however, the issue will be how to pull the capsule off the surface and retrieve it safely.

Currently a group of people are developing a projector method (C) and its possible designs. The basic idea is to project a 5-10 grams projectile toward the asteroid's surface with several hundreds [m/s] velocity inside the sampler horn. We expect this provides enough energy to crash the surface and the rebounding particles, or ejecta will be collected at the top corner of the horn. Since the sampling by the projector system will complete very quickly, the spacecraft is required to maintain the sampler contact for very short while, say 2-3 seconds, on the surface of the asteroid. This point is very favorable to our touch-down scenario.

2.4 Sampling Sequence

The gravitational force of the asteroid is very weak, estimated as one ten-thousandth of the earth gravity or less, the situation is therefore not that the explorer makes "landing" or "standing" on its surface but it does "rendezvous" and "berthing" in the free-flying environment. Assuming that MUSES-C takes the projection & crash method (Figure 2(C)) for sampling, we can summarize the sampling scenario as

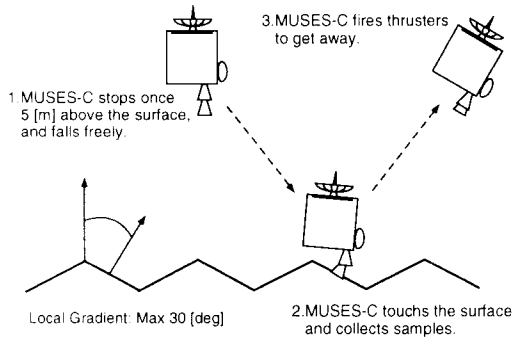

Figure 3: Sampling Sequence of MUSES-C

follows (see Figure 3):

1. The MUSES-C spacecraft makes rendezvous with the asteroid and descends to a point of interest.

2. About 5 [m] distance from the surface, MUSES-C is controlled its descending velocity to zero (hovering by thrusters,) then the thrusters are turned off to freely fall down on the surface. This will result 0.1 [m/s] vertical velocity at the surface contact.

3. The sampler horn, a contact probe is compliantly mounted on the spacecraft main body. The compliance works to reduce the contact impulse and extend the contact period.

4. While the endtip of the sampler horn stays on the surface, a projector is triggered and samples (ejecta) are collected inside the horn.

5. Thruster propulsion will follow immediately after the sampling, to get the spacecraft away from the surface. Note that thruster propulsion should turn on only after the sampling to prevent the contamination of the samples.

3 Modeling

3.1 Free-Flying Dynamics

To discuss flying or floating robot dynamics, we consider a general model that a robotic spacecraft has plural arms including solar paddles, reaction wheels or other appendages. Such a spacecraft is modeled by a chain of free-floating links in a tree configuration consisting of $n+1$ rigid bodies, connected with n articulated joints. Assume that ℓ pieces of arms are mounted on the main body, and the arm k has n_k pieces of links, then $n = \sum_{k=1}^{\ell} n_k$. An example with a single arm is depicted in Figure 4.

Flexible arms or solar paddles can be treated as segmented virtual rigid links connected with elastic

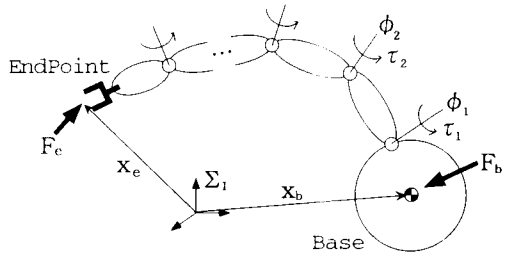

Figure 4: Free-flying robot system with a single arm

hinges. The flexibility yields elastic forces on the virtual hinges according to their virtual deformation. In this paper, we do discuss the compliance and deformation of the sampler horn, but do not discuss the flexibility of solar paddles or other appendages to avoid complexity.

We assume that the system freely floats in the inertial space, and no orbital motion is considered.

Let us define the following coordinates and driving forces applying on the system.

$\boldsymbol{x}_b$	$\in R^6$	: position/orientation of the base
$\boldsymbol{\phi}$	$\in R^n$	: joint angle of the arm
$\boldsymbol{x}_e$	$\in R^6$	: position/orientation of the endpoint
$\mathcal{F}_b$	$\in R^6$	: thruster force/moment on the base
$\boldsymbol{\tau}$	$\in R^n$	: joint torque of the arm
$\mathcal{F}_e$	$\in R^6$	: external force/moment on endpoint

Here we can obtain the equation of motion in the following form [2, 3, 4, 5]:

$$\begin{bmatrix} \boldsymbol{H}_b & \boldsymbol{H}_{bm} \\ \boldsymbol{H}_{bm}^T & \boldsymbol{H}_m \end{bmatrix} \begin{bmatrix} \ddot{\boldsymbol{x}}_b \\ \ddot{\boldsymbol{\phi}} \end{bmatrix} + \begin{bmatrix} \boldsymbol{c}_b \\ \boldsymbol{c}_m \end{bmatrix} = \begin{bmatrix} \mathcal{F}_b \\ \boldsymbol{\tau} \end{bmatrix} + \begin{bmatrix} \boldsymbol{J}_b^T \\ \boldsymbol{J}_m^T \end{bmatrix} \mathcal{F}_e \quad (1)$$

where

$$\boldsymbol{H}_b \in R^{6\times 6} \equiv \begin{bmatrix} w\boldsymbol{E} & w\tilde{\boldsymbol{r}}_{0g}^T \\ w\tilde{\boldsymbol{r}}_{0g} & \boldsymbol{H}_\omega \end{bmatrix} \quad (2)$$

$$\boldsymbol{H}_\omega \in R^{3\times 3} \equiv \sum_{k=1}^{\ell}\sum_{i=1}^{n_k} (\boldsymbol{I}_i^k + m_i^k \tilde{\boldsymbol{r}}_{0i}^{kT} \tilde{\boldsymbol{r}}_{0i}^k) + \boldsymbol{I}_0 \quad (3)$$

$$\boldsymbol{H}_m \in R^{n\times n} \equiv \sum_{k=1}^{\ell}\sum_{i=1}^{n_k} (\boldsymbol{J}_{Ri}^{kT} \boldsymbol{I}_i^k \boldsymbol{J}_{Ri}^k + m_i^k \boldsymbol{J}_{Ti}^{kT} \boldsymbol{J}_{Ti}^k) \quad (4)$$

$$\boldsymbol{H}_{bm} \in R^{6\times n} \equiv \begin{bmatrix} \boldsymbol{H}_{v\phi} \\ \boldsymbol{H}_{\omega\phi} \end{bmatrix} \quad (5)$$

$$\boldsymbol{H}_{v\phi} \in R^{3\times n} \equiv \sum_{k=1}^{\ell}\sum_{i=1}^{n_k} m_i^k \boldsymbol{J}_{Ti}^k \quad (6)$$

$$\boldsymbol{H}_{\omega\phi} \in R^{3\times n} \equiv \sum_{k=1}^{\ell}\sum_{i=1}^{n_k} (\boldsymbol{I}_i^k \boldsymbol{J}_{Ri}^k + m_i^k \tilde{\boldsymbol{r}}_{0i}^k \boldsymbol{J}_{Ti}^k) \quad (7)$$

$$\boldsymbol{J}_{Ti}^k \in R^{3\times n} \equiv [\boldsymbol{k}_1^k \times (\boldsymbol{r}_i^k - \boldsymbol{p}_1^k), \boldsymbol{k}_2^k \times (\boldsymbol{r}_i^k - \boldsymbol{p}_2^k), \ldots, \ldots, \boldsymbol{k}_i^k \times (\boldsymbol{r}_i^k - \boldsymbol{p}_i^K), \mathbf{o}, \ldots, \mathbf{o}] \quad (8)$$

$$\boldsymbol{J}^k_{Ri} \in R^{3\times n} \equiv [\boldsymbol{k}^k_1, \boldsymbol{k}^k_2, \ldots, \boldsymbol{k}^k_i, \mathbf{o}, \ldots, \mathbf{o}] \quad (9)$$

$$\boldsymbol{r}_{0g} \in R^3 \equiv \boldsymbol{r}_g - \boldsymbol{r}_0 \quad (10)$$

$$\boldsymbol{r}^k_{0i} \in R^3 \equiv \boldsymbol{r}^k_i - \boldsymbol{r}_0 \quad (11)$$

m^k_i : mass of link i of arm k
w : total mass of the system ($w = \sum_{k=1}^{\ell} \sum_{i=1}^{n_k} m_i$)
$\boldsymbol{r}^k_i$: position vector of centroid of link i of arm k
$\boldsymbol{p}^k_i$: position vector of joint i of arm k
$\boldsymbol{k}^k_i$: unit vector indicating joint axis direction of link i of arm k
$\boldsymbol{r}_0$: position vector of centroid of spacecraft base body
$\boldsymbol{r}_g$: position vector of a total centroid of the system
$\boldsymbol{c}_b, \boldsymbol{c}_m$: velocity dependent non-linear terms
$\boldsymbol{E}$: 3×3 identity matrix
and a tilde operator stands for a cross product such that $\tilde{\boldsymbol{r}}\boldsymbol{a} \equiv \boldsymbol{r} \times \boldsymbol{a}$. All position and velocity vectors are defined with respect to the inertial reference frame.

3.2 Contact Dynamics

We assume the contact happens only at defined endpoints. Note that MUSES-C does not have what is called manipulator arm, but the endpoint of the sampler horn, which is modeled as an articulated compliant arm, makes contact with an asteroid. The following discussion is on how to determine the contact force $\mathcal{F}_e$.

In literature, there are a few papers to deal with a dynamic model of rigid body collision with friction. A paper by Keller [6] and a book by Brach [7] are good references. Most of literature including the aboves deal with the relationship of momentum exchange and force-time product under the assumption of infinitesimal impact. However, the infinitesimal impact between two of single rigid bodies is a very idealized, special case. Eventually if the colliding body has elasticity, there occurs non-zero, finite-time period of contact. Or if the system is articulated and the connecting joints are compliant, the methods discussed for infinitesimal impact of a single rigid body cannot be applied. We may call such finite-time contact as *soft* contact against the infinitesimal impact as *hard* contact.

On MUSES-C we put a spring between the main body and the sampler horn. The spring is used to deploy the horn to stretch out from the the launch configuration, and it is more important to fit the front end of the horn to the uneven surface and absorb energy at the time of contact. Therefore we need to treat the "soft" contact problem to simulate the contact behavior of the spacecraft.

The dynamic motion of the free-flying multibody system is described by Equation (1) with the presence of the external forces $\mathcal{F}_e$. The magnitude of the forces is determined by the compliant deformation and friction of the contact surface.

Let us assume a point contact, then the contact moment is zero and the translational contact force $\boldsymbol{f}$ should be discussed. If we assume a model of elastic-plastic deformation in the normal (z) direction of the contact point, and Coulomb friction in the tangential directions (x and y), we have the following general expressions:

$$^c\boldsymbol{f}_z = K(\boldsymbol{d})^r + D(\dot{\boldsymbol{d}})^s, \quad (12)$$

$$^c\boldsymbol{f}_x \leq \mu \cos\eta \; ^c\boldsymbol{f}_z, \quad (13)$$

$$^c\boldsymbol{f}_y \leq \mu \sin\eta \; ^c\boldsymbol{f}_z, \quad (14)$$

where $\boldsymbol{d}$ is the depth of penetration and $\dot{\boldsymbol{d}}$ is its velocity. The left-superscript $\{\ ^c\ \}$ indicates the local coordinate frame located on the contact point. Also, μ is *the coefficient of friction* and η is the angle defined by

$$\tan\eta = \frac{^c\boldsymbol{v}_{cy}}{^c\boldsymbol{v}_{cx}}. \quad (15)$$

There are number of discussions and still open questions on the above equations in the points that what numbers should be used for K, D, r and s, and how to find a consistent solution from inequality of the friction model. Here in this paper, we take an approach featured by a) a linear spring-damper model for the deformation mechanics, say $r = s = 1$, b) experimental estimation of K, D as is reported in [8]. And c) we take a special care on the treatment of frictional force, which may easily yield physically impossible solutions that is called *negative energy loss* by Brach [7].

4 Simulation

4.1 Model Parameters

Figure 5 depicts a drawing of MUSES-C used for the simulation. The kinematic and dynamic parameters of main components are listed in Table 1.

The sampler horn is assumed compliant in vertical (longitudinal) direction, but constraint in other directions.

The attaching point of the sampler horn is far away from the centroid, or the inertial principle axis of the main body. This off-axial attachment yields significant moment then angular motion to the main body due to the contact impulse, as will be seen in the simulation results later. However, a connecter interface with a launching rocket booster takes place in the center of this surface, then there is no room to mount the sampling horn on axis.

The surface of the asteroid is assumed with same or similar hardness and damping of firebricks. The parameters of the firebrick we identified are used in the simulation. The surface is assumed flat and horizontal.

Table 2 Simulation results: contact force, time and rebounding velocities

	With horn compliance			Without horn compliance
	$v_x = 0.08$ [m/s]	$v_x = 0.0$ [m/s]	$v_x = -0.08$ [m/s]	$v_x = 0.0$ [m/s]
V_x [m/s]	0.146	0.086	0.018	-0.010
V_y [m/s]	-0.004	-0.006	-0.007	-0.004
V_z [m/s]	0.032	0.066	0.093	0.064
ω_x [deg/s]	0.069	0.077	0.086	0.135
ω_y [deg/s]	1.934	1.169	0.359	1.599
ω_z [deg/s]	0.0123	-0.005	-0.021	0.017
f_{max} [N]	15.304	17.962	20.571	136.360
t_c [sec]	6.690	6.365	6.150	0.785

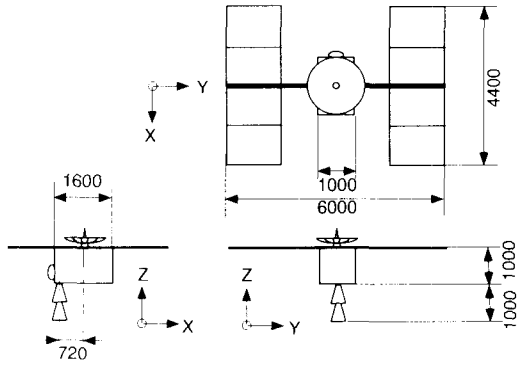

Figure 5: A drawing of MUSES-C used for simulation. Note that this is not a final configuration, which is currently under discussion as of June 1998.

Table 1 Simulation Parameters

mass of main body [kg]	m_0	409
moment of inertia [kg·m^2]	$I_{0_{xx}}$	300
	$I_{0_{yy}}$	230
	$I_{0_{zz}}$	430
attaching point of the sampler	d_x	-0.72
horn from the centroid	d_y	0.02
of main body [m]	d_z	-0.50
mass of sampler horn [kg]	m_1	1.0
moment of inertia [kg·m^2]	$I_{1_{xx}}$	1.0
	$I_{1_{yy}}$	1.0
	$I_{1_{zz}}$	1.0
compliance of the horn [N/m]	K_s	100
damping of the horn [Ns/m]	D_s	4.3
compliance of the asteroid [N/m]	K_w	10000
damping of the asteroid [Ns/m]	D_w	17.0
friction coefficient	μ	0.5
inclination of the surface [deg]	θ	0

4.2 Reaction of the Projector and Thrusters

The reaction of the projector and the gas-jet thrusters are other sources of external force on the main body than the contact impulse. The reaction of the projector is estimated to yield 3 [Nms]. Twelve of 22 [N] thrusters are mounted on the main body and four of them can be used to lift-off from the asteroid. However in the following simulation, these forces are not accounted, in order to see the nature of the physical contact and rebound.

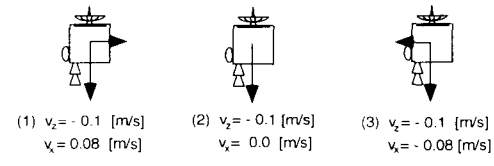

Figure 6: Three cases of contact velocity

4.3 Contact Velocity

The nominal contact velocity in vertical (z) direction is -0.1 [m/s]. The horizontal velocity, however, may be more difficult to control. This is because the height (vertical distance) can be measured by a ranging sensor, but there is not an easy way to measure the horizontal distance. Then we set a design interface for horizontal motion control to allow plus-minus 0.08 [m/s]. In the simulation, we evaluate three cases of contact velocity as shown in Figure 6.

4.4 Contact Force and Rebounding Motion

Figures 7 show an example of the simulation, where the contact forces, the horn-tip positions, and the attitude of spacecraft are displayed. As a parametric study, the rebounding (lift-off) velocities, the maximum contact force f_{max}, and the contact duration time t_c are compared as listed in Table 2.

The right column is the result without horn compliance to be compared with other three. It is clearly shown that the vertical (longitudinal) compliance in the sampler horn is very effective to reduce the con-

tact impulse and extend the contact duration.

All results show significant rotation around y axis. This is due to the moment of the off-axial horn attachment. This rotation is very serious especially when the spacecraft has horizontal velocity in $+x$ direction before the contact, because this horizontal motion accelerates the pitch rotation. Figure 8 depicts an animated motion in such a critical case. We should carefully consider solutions to avoid this case. On the other hand, if the spacecraft has horizontal velocity in $-x$ direction before the contact, the moment by the off-axial horn and the moment by the horizontal velocity will cancel each others, thus yield smaller rotation.

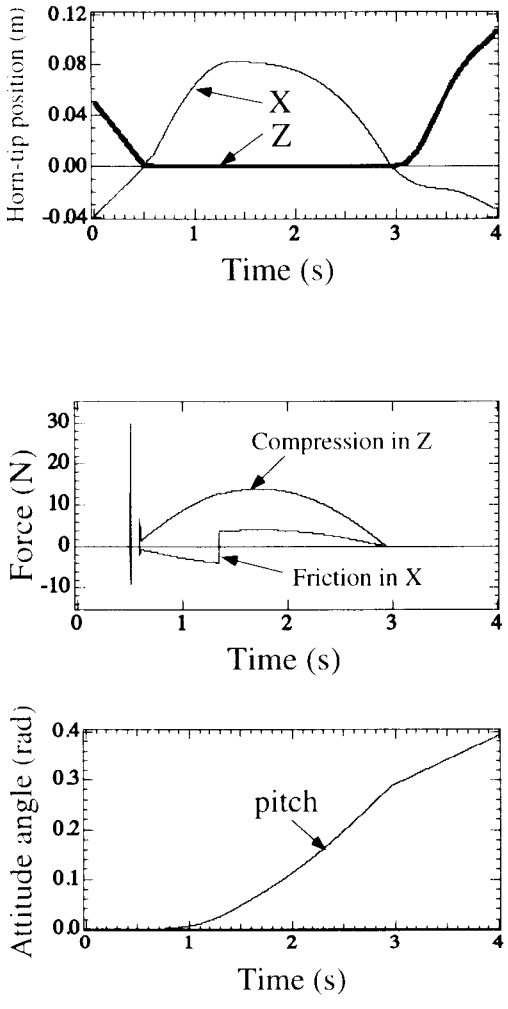

Figure 7: Simulation: a set of force/motion profile

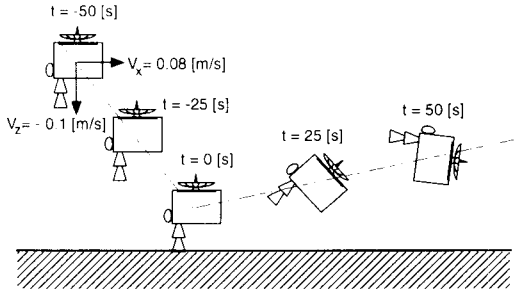

Figure 8: Simulation results of a critical situation

5 Conclusion

In this paper, we discussed the dynamics simulation of the MUSES-C spacecraft for asteroid sampling, from the free-flying and contact dynamics point of view. A mathematical model to deal with free-flying and contact dynamics is developed. Then the dynamics simulations are carried out for feasible touchdown conditions. As a result of the simulation, we find the longitudinal compliance in the sampler horn is effective, and point out a critical situation due to the off-axial attachment of the horn. We need to carefully design the sampling sequence and control procedure to avoid such hazardous, and clarify safety margins by further simulations.

References

[1] *A Proposal of the Asteroid Sample Return Mission: MUSES-C*, The Institute of Space and Astronautical Science, 1996. (in Japanese)

[2] *Space Robotics: Dynamics and Control*, edited by Xu and Kanade, Kluwer Academic Publishers, 1993.

[3] R. Mukherjee and Y. Nakamura: "Formulation and Efficient Computation of Inverse Dynamics of Space Robots," *IEEE Trans. on Robotics and Automation*, vol.8, no.3, pp.400–406, 1992.

[4] Y. Yokokoji, T. Toyoshima, and T. Yoshikawa: "Efficient Computational Algorithms for Trajectory Control of Free-Flying Space Robots with Multiple Arms," *IEEE Trans. on Robotics and Automation*, vol.9, no.5, pp.571–580, 1993.

[5] K. Yoshida: "A General Formulation for Under-Actuated Manipulators," *Proc. 1997 IEEE/RSJ Int. Conf. on Intelligent Robots and Syatems*, pp.1651–1957, Grenoble, France, 1997.

[6] J. B. Keller: "Impact With Friction," *ASME J. of Applied Mechanics*, vol.53, no.1, pp.1–4, 1986.

[7] R. M. Brach: *Mechanical Impact Dynamics: Rigid Body Collisions*, John Wiley & Sons, 1991.

[8] K. Yoshida and T. Hiraoka: "Touch Down Simulation of the MUSES-C Satellite for Asteroid Sampling," *1998 AIAA Modeling and Simulation Technologies Conference*, AIAA 98-4376, pp.1–7, Boston, MA, 1998.